Plasma Panel Detectors for Ionizing Particles

R. Ball[1], J. R. Beene[2], Y. Benhammou[3], E. H. Bentefour[4], J. W. Chapman[1], E. Etzion[3], C. Ferretti[1], P. S. Friedman[5], D. S. Levin[1], M. Ben Moshe[3], Y. Silver[3], R. L. Varner[2], C. Weaverdyck[1], and B. Zhou[1]

1. Department of Physics, University of Michigan, Ann Arbor, MI 48109 USA; 2. Physics Division, Oak Ridge National Laboratory, Oak Ridge, TN 37831 USA; 3. School of Physics and Astronomy, Tel Aviv University, Tel Aviv 69978 Israel; 4. Ion Beam Applications S. A., Louvain La Neuve, B-1348 Belgium; 5. Integrated Sensors, LLC, Ottawa Hills, OH 43606 USA (telephone: 419-536-3212, e-mail: peter@isensors.net).

Abstract–**The plasma panel sensor (PPS) is conceived as an inherently digital, high gain, novel variant of micropattern gas detectors inspired by many operational and fabrication principles common to plasma display panels (PDPs). The PPS is comprised of a dense array of small, plasma discharge, gas cells within a hermetically-sealed glass panel, and is assembled from non-reactive, intrinsically radiation-hard materials such as glass substrates, metal electrodes and mostly inert gas mixtures. The PPS offers the potential to provide low cost large area ionizing radiation detectors with high granularity, spatial resolution and fast response time. We are developing the technology to fabricate these devices with low mass and small thickness, using gas gaps of at least a few hundred micrometers. Prototype devices demonstrate a spatial resolution of about 300 μm with 1 mm granularity.**
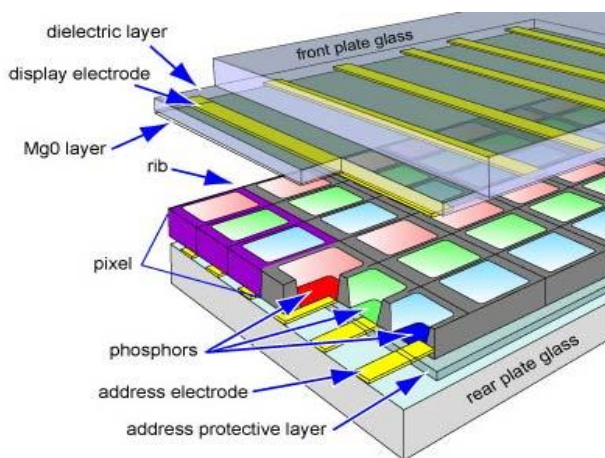
I. INTRODUCTION

THE plasma panel sensor (PPS) was conceived to take advantage of an existing, plasma-TV technology and manufacturing infrastructure and knowledge base for the production of large area, high definition, plasma display panels (PDPs). PDPs comprise millions of cells per square meter (see Fig. 1), each of which when provided with a signal pulse can initiate and sustain a plasma discharge to illuminate a phosphor. A PPS resembles a PDP, but is modified to detect gas ionization in the individual cells. A Geiger-mode discharge is initiated by ion-pairs created within a cell's gas volume by an incident ionizing photon or a traversing ionizing particle. The discharge is enabled by setting a bias voltage across the cell that exceeds the Paschen potential. The ionizing event creates an electron avalanche and possibly streamers that ultimately results in a large gas discharge whose amplitude is limited by the cell capacitance. The PPS discharge is terminated by a localized quench resistance. This impedance, combined with the cell capacitance, yields an RC time constant, or cell recovery time long enough that free charges and gas metastables in the cell volume are neutralized or deactivated. Depending upon the application, this resistance can be localized at each cell or for each chain of cells along one electrode line, as is the case for the prototype tests reported here.

Fig. 1. Typical PDP structure for plasma-TV panel.

Relative to a PDP, the cell configuration and fabrication process is simplified by the elimination of color phosphors, contrast enhancement and protective layers, rib structures, and thin-film secondary electron emitters (e.g. MgO). On the other hand the cell geometry must be tailored for high efficiency - meaning an adequate volume where ion-pairs can be created. Such high efficiency designs involving a deep cell structure combined with higher fill-factor are currently being designed and prototyped. This paper reports results conducted with low efficiency plasma displays. Unlike most other micropattern gaseous detectors, PPS devices can be hermetically-sealed and are fabricated using stable, non-reactive, inherently radiation-hard materials such as glass substrates, refractory metal electrodes and inert or stable gasses.

II. PPS POTENTIAL ATTRIBUTES

Plasma panel sensors potentially have a number of attributes that, with sufficient research and development support, could lead to a very attractive detector technology. The special attributes that distinguish this PPS technology are:

1. **Sparking and gain:** A recurrent problem with micro-pattern detectors which operate with gains of ~10^4 (and greater) is possible destructive sparking. The PPS is designed to be a higher gain, Geiger-mode device and, intrinsically immune from sparking. An inline current-limiting quench resistor associated with every PPS pixel immediately drops the voltage at discharge and terminates the current pulse.

1

2. **Longevity and radiation hardness:** PPS materials that form PDP television displays are glass, non-reactive refractory/metal electrodes and inert or non-corrosive gas mixtures. They contain no thin-film polymers or plastics used in other micropattern detectors, and no hydrocarbons that can degrade or outgas. All PPS materials are intrinsically rad hard.

3. **Hermetic gas containment:** PPS envelopes will be fabricated using the same industrial processes and hermetic glass seal materials used for PDPs. The glass panels are impermeable to atmospheric gases and no external gas system is required. Proven PDP lifetimes exceed 10^5 hours.

4. **Spatial resolution and granularity:** Mature photolithographic and ion-milling techniques are used to deposit electrodes with micron-level precision. Current manufacturing capability already exceeds this precision thus providing a direct path to higher resolution PPS devices. We have currently obtained using only low resolution, commercial off-the-shelf, modified PDPs, granularity of 1 mm and RMS resolutions of 300 μm.

5. **Fast response and high rates:** Signal development depends on gas avalanche and streamer formation over a narrow gap. These processes are intrinsically fast, on order of ns or less, depending on gas gap geometry, gas type, etc. Rate capability is determined by the cell recovery time. In tests using commercial PDPs with large capacitances, recovery times are ~O(10) μsec. With pixel densities from hundreds to thousands of cells/cm^2, the hit rate capability can potentially reach ~100 MHz/cm^2.

6. **Cost and scalability:** PPS detectors would benefit from the same fabrication processes, materials, and associated mechanical and electrical properties as large area PDPs – e.g. they would be lightweight and structurally rigid. Large size PDP display units exceeding 100 inch diagonal are commercially available. Current prices for 40-50 inch diagonal PDPs are less than \$0.15 inch^{-2} [10]. PPS readout electronics would be similar to those used in other high channel density, two coordinate detectors. The expected high gain of a PPS renders them intrinsically binary, possibly obviating an amplification stage and thus simplifying the front-end signal processing. Also because they are fabricated on glass substrates, high density, high speed electrode to integrated circuit interconnections can be achieved via low cost, chip-on-glass (COG) technology such as on PDPs and LCDs.

III. PPS DEVICE CONFIGURATIONS

A number of PPS device configurations have been considered [1]-[4] with several being investigated, but in all cases each pixel operates like an independent micro-Geiger counter, so the gas discharge can be initiated by either ionization of the gas, or by electrons emitted by a conversion layer in contact with the gas (e.g. for neutron detection) [5]. Our initial focus however, has been primarily on fabrication and lab tests of PPS devices derived directly from modified, commercially produced PDPs. These very thin gas gap devices (200-400 μm), although inherently inefficient, can detect

charged particles by direct gas ionization [6],[7]. They provide a versatile and cost effective test bed in which to evaluate and establish many PPS response characteristics. Our lab results have informed the design of a next generation PPS intended to have much higher intrinsic efficiency.

Fig. 2 shows a *columnar-discharge* PPS with an open-cell orthogonal X-Y electrode structure. "Open-cell" means that there is no rib enclosure surrounding each cell as shown in Fig. 1 for PDP TVs. The discharge occurs and, generally remains confined, in the volume defined by the intersection of the front column electrodes (e.g. high voltage -cathodes) and the back row electrodes (e.g. sense anodes) as shown in Fig. 2. The discharge/gas gap in these PPS-from-modified-PDP devices is typically a few hundred micrometers. The electrode widths range from about 0.4 to 1.3 mm.
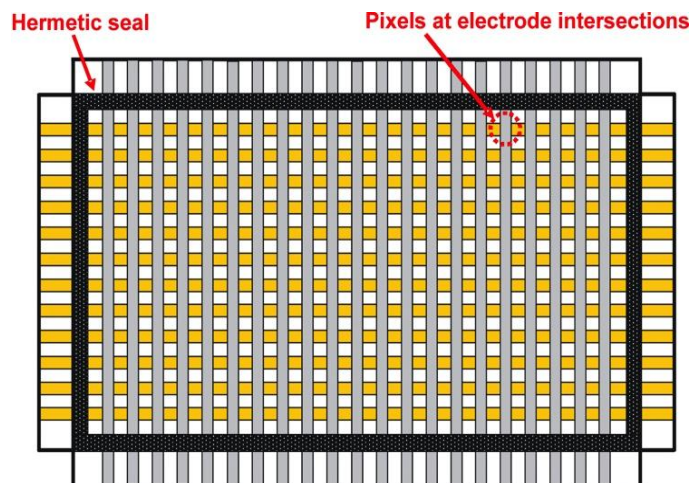

Fig. 2. Sketch of columnar-discharge PPS electrode structure. Dimensions range from 10-30 cm long, electrode pitch varies from 0.6 to 2.5 mm. Gas gaps are 200-400 μm.

Fig. 3 shows an example of a columnar-discharge PPS test panel having the orthogonal electrode structure in Fig. 2, after modifying a commercial 2-electrode, DC-type, glass PDP. The panel in Fig. 3 is attached to a removable aluminum frame for mechanical integrity, which is fitted with a sealed, high-vacuum, shut-off valve to allow multiple fills of different gas mixtures and pressures. The panel active area is 8.1 cm x 32.5 cm, has 3 mm thick float glass substrates and uses either transparent SnO$_2$ or Ni column high voltage electrodes (i.e. cathodes), and Ni back row sense anodes. The electrode pitch of the panel shown is 2.5 mm. Other tested devices have 1 mm electrode pitch. The results reported here are from both 2.5 mm and 1 mm panels. These panels undergo a systematic bake-out and gas fill procedure before being operated as detectors. In this configuration, with small gas gaps (~ 400 μm) relative to the 1.3 mm electrode widths, the field between anode and cathode is fairly uniform, as determined by COMSOL modeling [8]. A readout electronics card mounts on the horizontal anode lines and the signal is picked off using a 50 ohm termination resistance. A high voltage bus feeds the vertical cathode lines via a single quench resistance per line.

Fig. 3. PPS "refillable" test panel.

The refillable PPS test panel in Fig. 3 has proven more durable than initially expected, as it typically holds a given gas mixture for months without any observed change in performance. In fact our best test panel to date continues to be operational one year after the shut-off valve was closed. By being able to use the same panel with different gas mixtures, we can study the effect of gas composition and pressure completely isolated from any uncertainty associated with panel-to-panel variations in: discharge and/or gas gap, electrode line width, thickness and surface condition, substrate thickness and dielectric surface variation, etc. We have prepared similarly constructed panels to Fig. 3, but with a pixel pitch of 1.0 mm and 0.6 mm.

IV. CURRENT EXPERIMENTAL EFFORT

Our collaboration has constructed two test benches, one at the University of Michigan and the other at Tel Aviv University. Each site includes a gas delivery system, a triggering system, and a data acquisition (DAQ) system. At these labs, we use beta-emitters, Sr-90 and Ru-106, (max. electron energy of 2.3 MeV and 3.5 MeV) and cosmic-ray muons as our test radiation. We also have access to a ProCure medical proton beam accelerator near Chicago through an informal collaboration with Belgium proton beam therapy manufacturer Ion Beam Applications S.A. (IBA). We used their Model C235 accelerator to test our devices with a 226 MeV collimated proton beam using aperture diameters of both 1 mm and 10 mm. The triggering system for our lab-based experiments is done with a scintillator hodoscope, or relies on self-triggering. The proton test beam data were acquired with a PPS self-trigger.

The DAQ system is adapted from the Muon Spectrometer monitored drift tube readout electronics developed (in part by the University of Michigan) for the ATLAS experiment at the Large Hadron Collider. This system can acquire data using 24 channel readout cards with sub-nanosecond resolution. Additional readout methods include a 20 channel scaler and 16 channel fast waveform digitizer for pulse shape analysis.

V. SURVEY OF RECENT LAB RESULTS

We have investigated the PPS device response to a number of ionizing particle sources under different experimental conditions with various discharge gases. The discharge gases tested include: $Ar+CO_2$, $Ar+CF_4$, CF_4, SF_6 and Xe. For a few of them the pressures have ranged from about 200 to 700 torr, but here we mostly report results at a single pressure of 600 torr. The observed signals from all of the devices tested have had large amplitudes of at least several volts, so there has been a need for attenuation instead of amplification electronics. For each gas tested, the shape of the induced signals is uniform. The leading edge rise time for the current generation of panels is typically 1 to 2 ns (see Fig. 4). Not unexpectedly, the device performance has been shown to be very much gas dependent, with the operating voltages varying by more than 1000 volts for different gas mixtures in the same panel.

For all the sources noted above the signal pulses appear similar (see Fig. 4) for a given panel geometry, gas mixture, cathode voltage, and quench and signal resistors. In other words, the signal amplitude, rise time and duration do not appear to depend on the event causing the initial gas ionization. There is nothing surprising about this observation as the cells are being driven in the Geiger or gas breakdown mode.
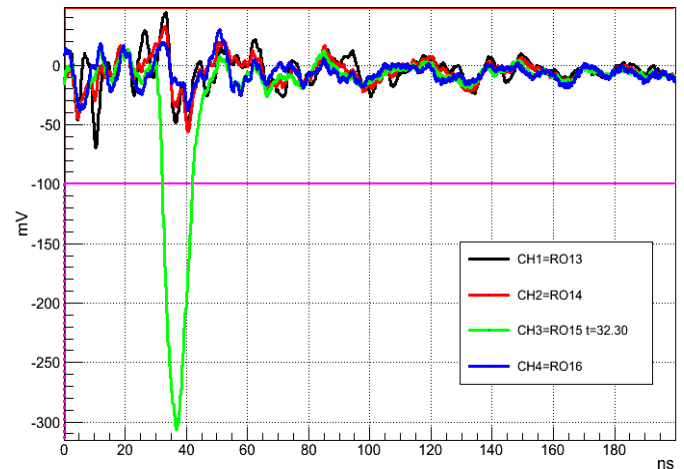

Fig. 4. Typical signal pulse for columnar-discharge PPS. The signal is attenuated by 40 db. Panel has 2.5 mm pitch electrode, 600 torr Xe, operated at 1120 V. Signal in green; the other colors represent nearest neighbor pixel lines.

Signal characteristics: A typical PPS gas discharge pulse, after attenuation, is shown in Fig. 4 from a panel similar to that in Fig. 3, filled with Xe at 600 torr, operated at 1120V. The signal is from a [106]Ru beta-source. The rise time was ~ 2 ns. Other gas mixtures yield ~1 ns rise times and pulse widths at half maximum ≤ 2 ns [7]. Depending on the specific panel dimensions, gas and discharge high voltage, signal amplitudes can range from from a couple of volts to tens of volts. These large amplitudes result from the effective discharge capacitance for these PPS panels including stray capacitance contributions from neighboring electrodes as determined both experimentally and from SPICE simulations [1],[9].

3

Effect of quench resistance: For a given panel and gas mixture, we can generate a PPS *characteristic response curve* of dependence of the rate on the high voltage quench resistance, as shown in Fig. 5. The panel response is the rate of hits detected and is plotted as a function of the reciprocal of the line quench resistor.
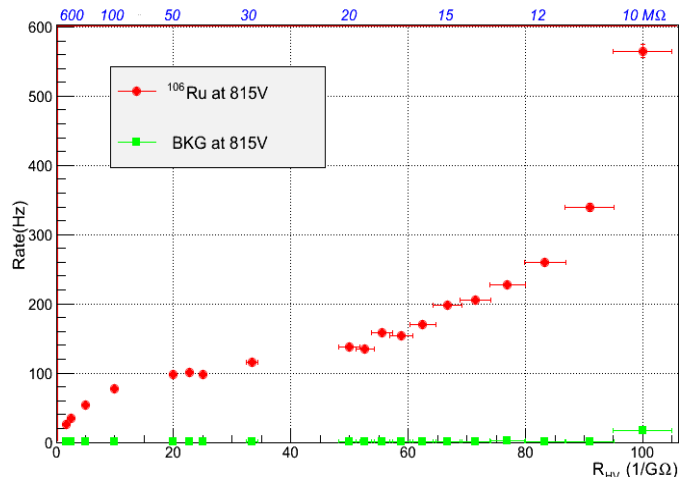

Fig. 5. PPS response exposed to radioactive beta source in red. Hit rate of 4 readout lines and one high voltage line versus 1/quench resistance. The lower x axis indicates the inverse resistance. The upper X axis indicates the quench resistance. Green data points are the hit rate without the source.

In order to be representative of the panel, the data of this curve are the response sum over several cells on a given cathode line so as to be indicative of the average panel performance for a given line quench resistor. For the data shown in Fig. 5, the panel gas was 1% CO_2 in Ar at 600 torr and was operated at 815 volts. The radiation source was ^{106}Ru and the hits were collected on a single high voltage line (#110), across four readout lines (RO = 3-6). The quench resistors covered the range from 10 to 600 MΩ.

As suggested by Fig. 5, the PPS characteristic response curve can be analyzed as consisting of three different response regions. For very high quench resistance values, 100 to 600 MΩ, the PPS response rate drops quickly because a high RC time constant means that each high voltage line is dead for a longer time and the maximum line rate is limited by the recovery frequency (order of magnitude ~ 1/RC). At the other end of the curve, 10 to 25 MΩ, the PPS response rate increases quickly as the quench resistance drops. This is caused by a small RC time constant that allows the high voltage to return to discharge potential before all of the charged species in the cell can be neutralized. This, in turn, leads to after-pulses due to regeneration resulting in exaggerated count rates. A major contributor to such after-pulses is gaseous metastable species that also have not yet had enough time to decay. Finally there is a nearly flat range of "moderate" quench resistance values and moderate RC time constants, in which we see minimal rate dependence on the quench resistor value. For the panel in Fig. 5, the response rate in this region is ~ 100 Hz.

Spontaneous backgrounds: Another significant result illustrated in Fig. 5 is the PPS response with no source present.

The measured background rate is minimal across the entire quench resistance region. This behavior is similar to the very low background rates observed over a large range of signal producing voltages that we reported previously for a panel with transparent SnO_2 cathodes and filled with CF_4 at 500 torr [6]. In general, PPS devices appear to have low background counts. Although low background count rates in the absence of an efficiency measurement can be misleading, we consider the measured low rates to be a promising indication of good performance.

Arrival time: In addition to the low background rates discussed above, we have shown for panels such as in Fig. 3, filled with fluorinated discharge gases, that the arrival time jitter (σ) as measured using cosmic-ray muons is $\leq$ 5 ns [1], [6], as shown in Fig 6.
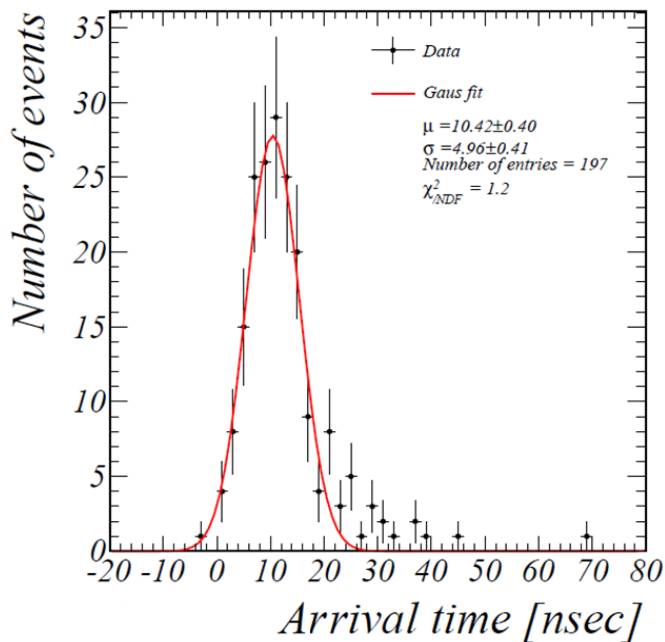

Fig. 6: Arrival time distribution of cosmic ray muons with respect to scintillator trigger signal. Gaussian fit width is about 5 ns using SF_6 at 200 torr.

The same type of panel in Fig. 3 was deployed in the CERN H8 test beam of 180 GeV muons. In this test, the panel was filled with Ar/CO_2 (93%, 7%) at 600 torr. Over 600 muons were collected and their arrival time distribution is shown in Fig. 7.
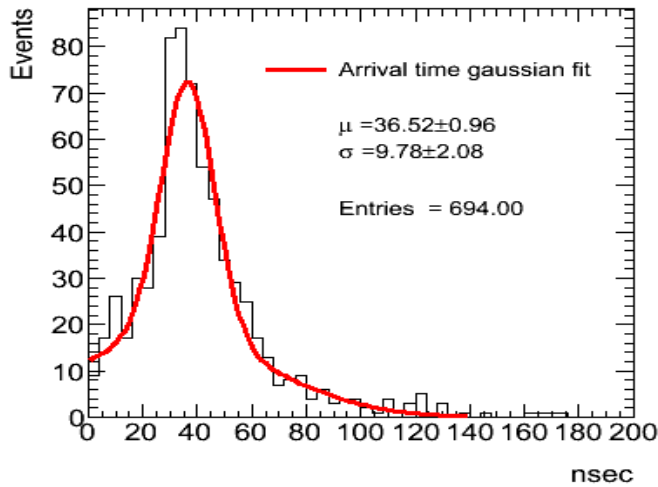
Fig. 7: Arrival time distribution of 180 GeV muons with respect to scintillator trigger signal. Data acquired in CERN H8 test beam. Fit is double Gaussian. Jitter is about 10 ns using Ar/CO_2 (7%) gas at 600 torr.

Spatial resolution and granularity: An important PPS parameter is the device position resolution. We measured it acquiring data while translating a "collimated" [106]Ru beta-source using a 1.25 mm wide graphite slit (20 mm thick) in 1.0 mm increments across the sense electrodes in the PPS panels with 2.5 mm and 1 mm electrode pitch. These panels were respectively filled with the 1% CO_2 and 10% CF_4 in Ar gas mixtures operated at 880 and 890 volts. The plot in Fig. 8 shows a typical hit distribution for the 1.00± 0.01 mm pitch panel. The RMS spread is 1.5 mm, a convolution of the source spread and the intrinsic panel resolution. The source Gaussian spread is modeled from a GEANT4 [11] simulation and is 1.1 mm (although the FWTM is 6.5 mm) as shown in Fig. 12. We estimate that the intrinsic resolution is consistent with the 1 mm electrode pitch- having an RMS of ~300 μm. Fig. 9 and Fig. 10 show the Gaussian means of the hit distributions vs. the source position for the 2.5 mm and 1 mm pitch panels respectively. We obtain slopes of 0.39 ± 0.01 mm^{-1} and 0.98 ± 0.01 mm^{-1}, both consistent with the electrode pitch.
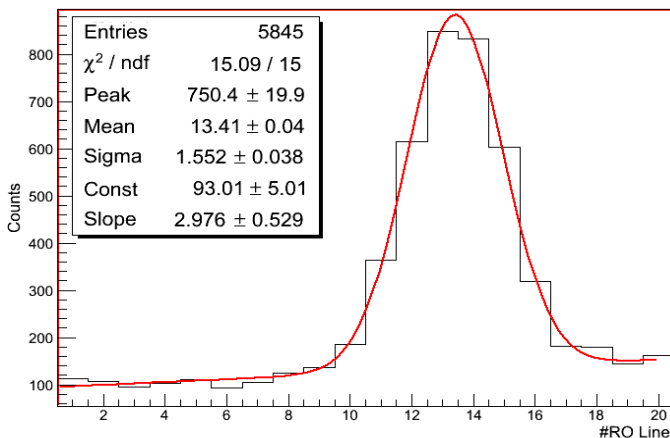

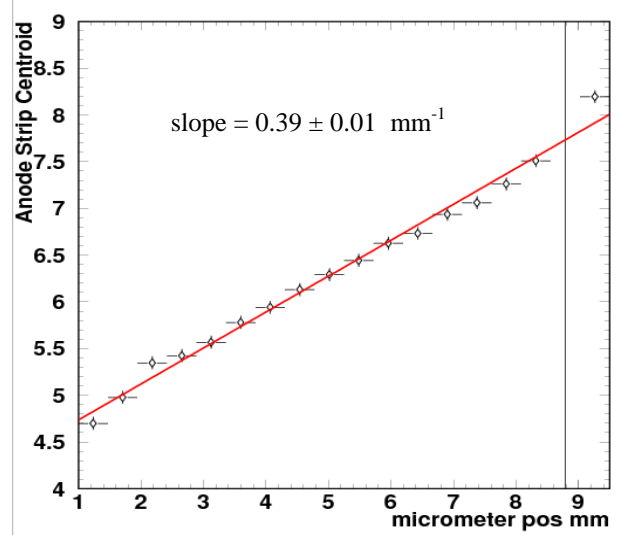Fig. 8 Distribution of hits (along readout lines) from beta source on panel with 1.0 mm electrode pitch.

Fig. 9 Beta-scan position resolution measurements for a panel with 2.5 mm electrode pitch, and Ar / 1% CO_2 gas mixture.
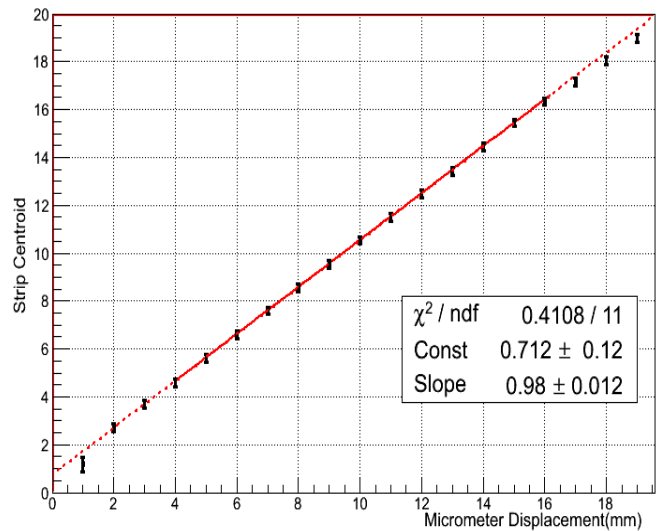

Fig. 10. Beta-scan position resolution measurements for a panel with 1.0 mm electrode pitch and Ar / 10% CF_4 gas mixture.

A GEANT4 simulation is used to evaluate the contribution to the position resolution of the spreading/scattering of source emitted electrons. The incoming electrons are described by a stream of beta particles emanating out of the [106]Ru source and traveling through the 20 mm long air gap of the 1.25 mm wide graphite collimator and then through the 2.25 mm thick glass substrates of the PPS. A total of 1,000,000 tracks were run yielding the representation of a sub-sample of 100 random tracks shown in Fig. 11. Most of the scattering and absorption of betas occur in the PPS front glass substrate with very few betas exiting the back glass substrate.
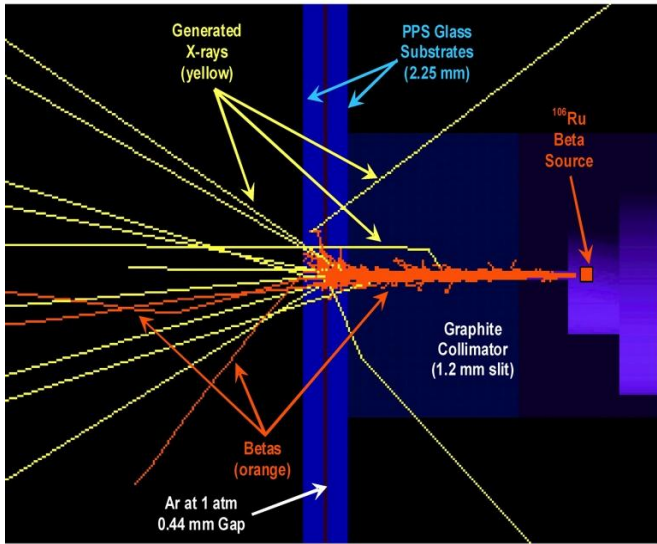
Fig. 11. GEANT4 beta scattering simulation with ^{106}Ru source.

The initial 1.25 mm collimated beam of beta particles has a scattering full width at half maximum of about 2.6 mm at the discharge gas volume, with long non-Gaussian tails, as shown in Fig. 12. In other words, the "collimated" beta beam inside the PPS illuminates approximately two adjacent sense electrodes on each side of the targeted electrode under the graphite slit. Given this incident particle dispersion, the fact that we are able to resolve the beam centroid steps to less than the PPS cell pitch of 1.0 mm bodes very well for the potential position resolution of these devices. In this regard we are currently in the process of fabricating next-generation PPS devices with a cover plate thickness of 0.50 mm (compared to the current 2.25 mm thickness), and eventually plan to fabricate even thinner devices with an electrode pitch of ~ 0.15 mm. We expect that such PPS devices should have a position resolution of $\leq 50\ \mu m$.

Proton beam tests: We performed our first beam experiments with an IBA-C235 proton beam accelerator used for proton therapy (i.e. treatment of cancer) in March 2012. Fig. 13 (top) shows the number of hits per channel during a position scan using an intense (i.e. > MHz) 1 mm diameter, 226 MeV proton beam for 16 sequential runs in which the panel in Fig. 3 was shifted in each run by ~ 1 mm increments relative to the fixed position proton beam. Each bin is a single data channel for a sense-electrode line. Fig. 13 (bottom) shows the reconstructed position centroid of the "hit" map from Fig. 13 (top) versus the PPS relative displacement in millimeters with respect to the initial position. The position centroid for each run is based on the weighted average over 3 bins around the peak. As with the beta position resolution scans in Fig. 9 and 10, the resulting slope of the linear fit (p1 in the legend) establishes that the panel was able to reproduce the proton beam position.
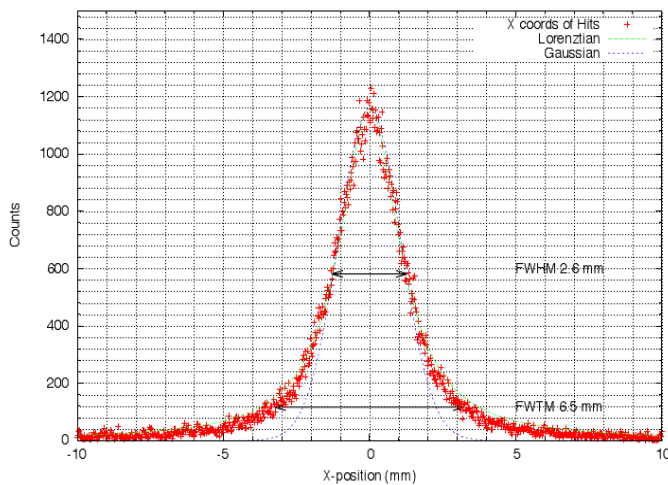

Fig. 12 GEANT4 simulation showing the expected distribution of betas from the slit collimated ^{106}Ru source inside the PPS cell gas volume. The width of the distribution is comparable to the measured distribution shown in Fig. 8.
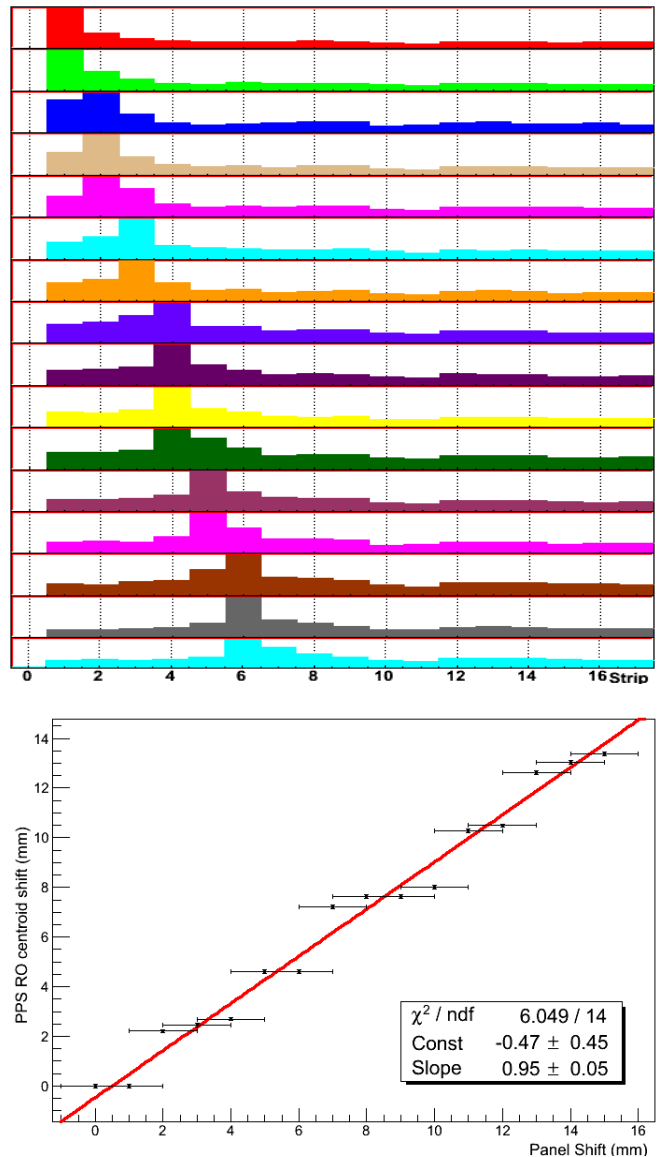
Fig. 13. Position scan measurements with an intense 1 mm diameter, 226 MeV proton beam used for cancer therapy. Top: raw hit distributions. Bottom: fit to centroids.

6

The steps observed in the Fig. 13 (bottom) data are presumed to be caused by the intense beam saturating the central pixels. This saturation derives from the deliberately long time constants chosen for this first proton beam test.

Saturation tests: To further investigate PPS saturation the response to the simultaneous exposure to two sources was measured in an experiment as follows: Four adjacent 32 cm long signal readout (RO) lines (i.e. sense row electrodes) were connected to discriminators whose outputs were OR'ed and then their combined signal rates were measured with a rate counter. High voltage was applied to two transverse column electrodes (i.e. cathodes) at varying distances from one another. Specifically, high voltage was applied always to one fixed line (#110) while the second line receiving high voltage was allowed to vary from #100 up to #110 (see Fig. 14).

Fig. 15. Ratio of the rate from two simultaneous sources divided by the sum of the two rates from the same sources separately.
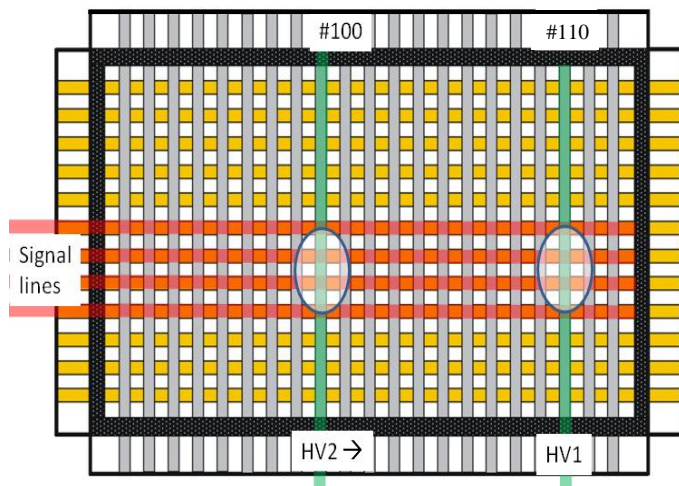

Fig. 14. Configuration for double source test. Shaded regions show approximate location of radioactive beta sources. The line labeled HV2 is incremented from left to right towards HV1.

The intersections of the isolated high voltage electrodes with the four readout electrodes constituted the active pixels in this test. Each set of four pixels was exposed at first separately, and then simultaneously to two *partially* collimated sources (^{90}Sr and ^{106}Ru) yielding approximately similar rates of betas entering the gas gap region. These sources were positioned, one below the panel and one above, over the active pixels as indicated by the two oval shaded regions in Fig. 14. The second source position was incremented from left to right across the panel starting from line #100. As in the proton beam test, a large quench resistance was deliberately selected in order to produce long cell recovery times close to the saturation value along the high voltage line. The rates of the two groups of pixels were measured when exposed independently and then simultaneously to the two sources.
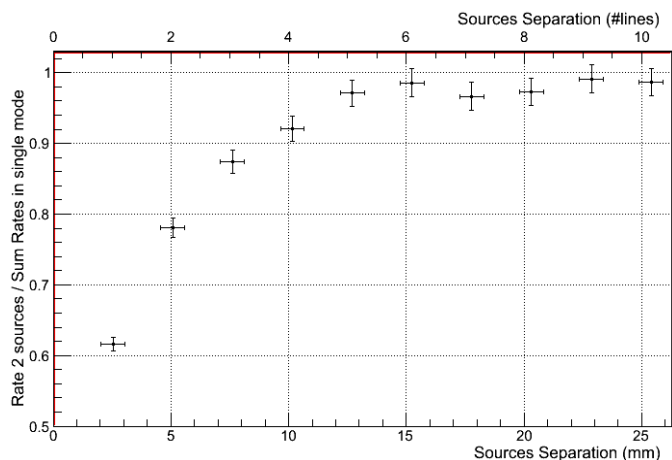
The rate of the four RO lines measured when both sources are simultaneously used equals the linear sum of the rates from two sources when measured individually over nearly the entire width of the panel, which results in the near unity ratio across most of Fig 15. Significant deviations are observed when the two sources are brought within a few lines of each other; in particular when their separation falls below 10 mm - i.e. within 4 lines. As discussed previously, each source has a scattering full width half maximum in the PPS of about 2.6 mm (actually the dispersion is slightly worse than in the GEANT4 simulation for Fig. 11 because the two sources were only *partially* collimated and the glass was 1 mm thicker). From Fig. 15 we observe that starting from a separation distance of 7.5 mm (i.e. line #107 in Fig. 14), the double source rate decreases below 90% of the sum of the two rates in single mode. When a single source is used over a high voltage line, the total rate is increased by betas scattered over another line if it is close enough. But when both sources are used at the same time, and both lines are respectively saturated by their corresponding source, then when both sources are close enough to overlap in terms of their scattering radius (e.g. with sources on lines #107 and #110) the rate increment due to the overlapping scattered electrons cannot happen. Hence the reduced ratio observed in Fig. 15 (i.e. starting at line #106 and dropping below 90% for line #107). The initial experimental results of the double radiation source tests indicate that the saturation effect is quite limited to within about 2 nearest neighbors. Our new generation of PPS structures, which are being fabricated with a 0.50 mm cover plate thickness and with 12% lower substrate density, should result in much less scattering of incident beta radiation, as well as less capacitive coupling and, due to a quench resistance at each pixel, also reduced saturation. This should thus allow further improvement in the resolution of adjacent cell hits by separate sources.

VI. CONCLUSIONS

This paper describes the potential attributes of plasma panel sensors, a new gaseous detector that has the potential for inexpensive, large area coverage, high resolution, high

granularity, and fast timing response performance in an intense radiation environment. These detectors can exploit over four decades of plasma display panel development and manufacturing infrastructure. We have undertaken a program to develop these detectors in which the first generation prototypes are adapted directly form monochromatic plasma display panels. They can also be hermetically sealed, thus eliminating the complexity associated with a number of other micropattern gaseous detectors that require a continuous gas flow support system. However, even without a *hermetic* seal, we have developed a mechanical valve/seal system together with a panel baking and gas filling procedure that allows each panel to operate as a stable, portable test chamber for evaluating the PPS device performance as a function of the discharge gas mixture and pressure.

We have investigated a number of performance metrics using these inexpensive off-the-shelf commercial devices. The measurement of a PPS characteristic response curve of a panel (depending on its structure, on the gas mixture and on the bias voltage), allows one to select a quench resistance value to work in a region where the hit rate is stable. This is a first important step toward a good evaluation of the efficiency of the PPS.

We have demonstrated that high gain, fast time response, high spatial resolution and high granularity are achievable. The first prototype detectors have successfully measured high energy muons in a test beam and cosmic rays, intense protons in a cancer therapy beam, and betas from radioactive sources. These detectors have worked months after being filled with gas and valved off. Some of the test results, reported in this white paper, have informed the next generation plasma panel design, which is currently being fabricated.

As we transition to discharge cells with better cell physical and electrical isolation, a deeper drift space and higher fill factors we expect to achieve lower capacitance and faster discharge times in the sub-nanosecond range, very high position resolution, and excellent response to high luminosity sources. Deeper cells with longer interaction paths will dramatically increase efficiency.

REFERENCES

[1] Y. Silver *et al.*, "Development of a Plasma Panel Radiation Detector: Recent Progress and Key Issues", IEEE 2011 NSS-MIC (Valencia, Spain), Conf. Record, 1881-1885.

[2] R. Ball, *et al.*, "Progress in the Development of a Plasma Panel Detector", IEEE 2010 NSS-MIC (Knoxville, TN), Conf. Record, 1536-1539.

[3] P. S. Friedman, "A New Class of Low Cost, High Performance Radiation Detectors", IEEE 2005 NSS-MIC (Puerto Rico), Conf. Record, 2815-2822.

[4] Integrated Sensors, LLC has the following 11 patents – i.e. nine *issued* U.S. patents and two *issued* Japanese patents, with a dozen more U.S. and foreign patents pending on plasma panel radiation detectors: 7,332,726; 7,518,119; 7,564,039; 7,683,340; 7,696,485; 7,902,516; 7,982,191; 8,158,953; 8,389,946; and JP-5023057; JP-5023058.

[5] R. L. Varner., J. R. Beene and P. S. Friedman, "Gadolinium Thin Foils in a Plasma Panel Sensor as an Alternative to ^{3}He", IEEE Nuclear Science Symp & Medical Imaging Conf. (Knoxville, TN), NSS Conf. Record, 1130-1136 (2010).

[6] P. S. Friedman *et al.*, "Plasma Panel Detectors as Active Pixel Beam Monitors", Newport News, VA: Beam Instrumentation Workshop, April 2012, Proceedings of BIW12, Paper MOPG021 (in press).

[7] P. S. Friedman *et al.*, "Plasma Panel Sensors for Particle and Beam Detection", IEEE 2012 NSS-MIC (Anaheim), Conf. Record, 1775-1780.

[8] COMSOL Multiphysics, http://www.comsol.com/products/multiphysics (COMSOL Inc.).

[9] L. W. Nagel and D. O. Pederson, SPICE (Simulation Program with Integrated Circuit Emphasis), Memorandum No. ERL-M382, Univ. of California, Berkeley (Apr. 1973).

[10] Price Trend Summary Report: Wholesale PDP panel prices for Feb. 2011, *Displaybank* (March 2011) updated Nov 2012 for retail prices on 50-51 inch PDPs (i.e. 1080p HDTVs from LG and Samsung).

[11] Agostinelli, S.; Allison, J.; Amako, K.; Apostolakis, J.; Araujo, H.; Arce, P.; Asai, M.; Axen, D. et al. (2003). "Geant4—a simulation toolkit". *Nuclear Instruments and Methods in Physics Research Section A: Accelerators, Spectrometers, Detectors and Associated Equipment* **506** (3): 250. doi:10.1016/S0168-9002(03)01368-8